Rakenteiden Mekaniikka (Journal of Structural Mechanics)
Vol. 44, No 3, 2011, pp. 231 – 242

On the self-excited vibrations of a viscoelastically covered cylinder in rolling contact using FE method

Anssi T. Karttunen and Raimo von Hertzen

Summary. As a result of ever-increasing speeds, the self-excited vibration of polymer-covered cylinders in rolling contact is becoming a more serious problem in many industrial processes. The vibration is generated by the viscoelastic behavior of the polymer covers. In this work, this vibration phenomenon, often referred to as barring, is studied using a two-dimensional rolling contact finite element model. The contact between two cylinders is modeled as a hard contact and the kinematic contact algorithm is used. The material parameters of the viscoelastic polymer cover of the other cylinder span a large relaxation spectrum. Readily available finite element software and tools are used for modeling and computations. The results show that strong barring vibration is a result of a resonance condition created in the rolling contact system. The vibration leads to the formation of a wave-like polygonal deformation pattern on the polymer-covered cylinder. The finite element model can provide detailed information on various phenomena, such as the nip waves, which have not been detected before by simplistic models.

Key words: polymer cover, viscoelasticity, barring, vibration, nip

Introduction

Contact vibrations of polymer-covered rolling cylinders have an adverse effect on the quality of the end product in industrial processes such as paper calendering and pressing. The vibrations originate from the viscoelastic behavior of the covers. Let us consider a two-cylinder system with a polymer cover on the other cylinder. The cover deforms viscoelastically within the contact area of the cylinders, that is, in the nip. For the most part, the deformations on the polymer cover recover quickly outside the nip, but the residual deformation acts as a time-delayed feedback as it returns to the nip after one revolution, causing self-excited vibration in the system. The vibration can lead to the formation of a wave-like deformation pattern on the cover of the cylinder. Furthermore, the surface deformations have a tendency to accumulate, which leads to severe, unstable vibration of the rolling system during its operation. In the present paper, the aim is to investigate this vibration phenomenon, often referred to as barring.

Classic papers related to contact vibrations deal with elastic bodies in rolling contact [1, 2]. The well-known methods to analyze rolling contact systems are summarized in Johnson's book, which covers also basic aspects of contact vibrations [3]. Another in-depth treatise on contact mechanics, concentrating more on three-dimensional bodies and numerical aspects, is Kalker's book [4]. In recent years, as the available computing power has increased, the focus has been on applying the finite and the boundary element methods in contact problems. For viscoelastic bodies rolling in contact see e.g. [5, 6, 7]. Most contact mechanical studies focus purely on the analysis of contact stresses. It is customary that the inertial effects are neglected and the vibration of the rolling bodies is

not of interest. There is a clear need for models which reach out towards inertia-related issues in rolling contact of viscoelastic bodies.

The self-excited vibration mechanism caused by viscoelastic cover behavior in rolling contact is not yet fully understood. The barring vibration has been studied primarily using 1D models [8, 9, 10, 11, 12, 13, 14]. Together these papers succeed in explaining important basic characteristics of barring. In addition, interesting experimental results related to the problem can be found in papers by Chinn and Vuoristo et al. [15, 16, 17]. Based on the 1D modeling approach, methods have been developed to diminish harmful vibrations in rolling contact systems [18, 19, 20, 21]. Although the vastly studied 1D models bear notable intelligence, from the point of view of multidimensional contact mechanics and viscoelasticity the 1D modeling approach is insufficient.

In a recent study, a step has been taken towards the right direction by using a proper 2D contact mechanical approach in modeling the nip contact of two cylinders [14]. Still, to model realistic material behavior, the relaxation spectrum of the viscoelastic material should be taken into account to a larger extent. Ultimately, any comprehensive analytical model leads to a rigorous set of equations for which it is impossible to find an analytical solution. Another possibility, utilized in this paper, is to approach the viscoelastic contact problem using the finite element method and tools which are already provided by up-to-date FE softwares. In this paper, for the purpose of elucidating the self-excited vibration mechanism, a 2D FE rolling contact model built using ABAQUS is studied.

Numerical model of a rolling contact system

General setup

The 2D two-cylinder system under investigation is shown in Fig. 1. The polymer-covered upper cylinder is rolling in frictionless contact with the lower cylinder. The angular velocities of the cylinders are given as time-dependent kinematic conditions. At the beginning of the simulation the cylinders are touching at a point. The contact is created by setting a vertical force to the center of the upper cylinder. The force increases linearly from zero to a constant value in a short period of time. Simultaneously, the cylinder also starts to rotate from rest to a desired angular velocity.

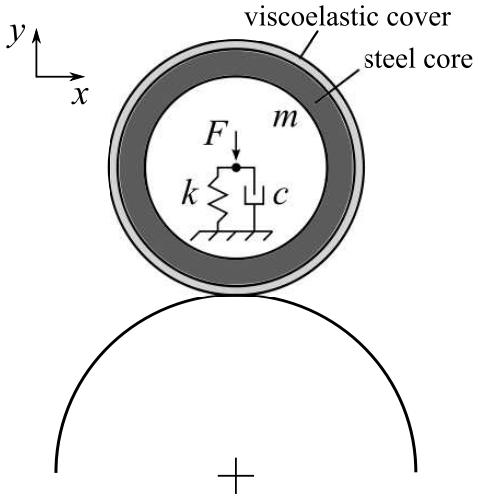

Figure 1. Schematic representation of the studied viscoelastically covered rolling contact system.

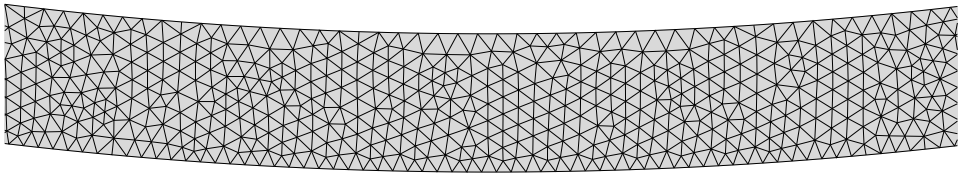

Figure 2. Mesh detail of the polymer cover.

The upper cylinder is supported by a linear spring-damper system and the cylinder is allowed to translate only in vertical direction. The steel core of the cylinder is modeled as rigid and the mass of the core is m. The polymer cover on the outer rim is viscoelastic. The lower cylinder is modeled as a massless rigid surface and the support of the cylinder is also rigid. The diameters of the upper and lower cylinder are 0.42 m (with cover) and 0.8 m, respectively. The thickness of the polymer cover is 7 mm. For the utilized plane strain model the width of the polymer cover in the longitudinal direction is set to 0.15 m. The polymer cover is modeled using three-node constant strain triangle (CST) finite elements[1] with linear viscoelastic constitutive behavior. The model has 27160 elements and a total of 15103 nodes, a detail of the mesh is shown in Fig. 2. The global element size has been set to 0.75 mm and the size on the inner edge to 1.0 mm.

Constitutive behavior of the viscoelastic polymer cover

Within the context of small strains, the constitutive equation for an isotropic viscoelastic material can be written in an hereditary integral form as

$$\boldsymbol{\sigma}(t) = \int_0^t 2G(t-\tau)\frac{d\boldsymbol{e}}{d\tau}d\tau + \mathbf{I}\int_0^t K(t-\tau)\frac{d\phi}{d\tau}d\tau \ , \tag{1}$$

where $\boldsymbol{\sigma}$ is the Cauchy stress tensor, G is the shear modulus, K is the bulk modulus, $\boldsymbol{e}$ is the deviatoric part of the strain, ϕ is the volumetric part of the strain, t is current time, τ is past time and $\mathbf{I}$ is the identity tensor [22].

The moduli can be represented in terms of the Prony series. For the shear modulus we get

$$G = G_0\left[1 - \sum_{i=1}^{N} g_i(1 - e^{-t/\tau_i^G})\right] \ , \tag{2}$$

where $g_i = G_i/G_0$ [22]. An analogous expression can be written for the bulk modulus. The deviatoric and volumetric parts are allowed to follow different relaxational behavior. The Prony representation corresponds to the solution of the classical Generalized Maxwell model of viscoelasticity. To perform numerical analysis, Eq. (1) needs to be integrated to the numerical solution, see [22]. The material parameters used for the polymer cover in this study are given in Table 1.

[1]ABAQUS/Explicit element type CPE3

Table 1. Material parameters of the viscoelastic polymer cover for the computations. The instantaneous Young's modulus $E_0 = 3.5166$ GPa and the Poisson's ratio $\nu = 0.35$. In the computations, the density of the polymer is scaled from $\rho = 1500$ kg/m^3 to $\rho = 9000$ kg/m^3. This halves the computation time without affecting the physical behavior of the system significantly.

i	1	2	3	4	5	6	7	8	9	10
g_i, k_i	.0291	.0292	.0329	.0341	.0365	.0397	.0363	.0410	.0423	.0408
τ_i^G, τ_i^K [s]	10^{-5}	10^{-4}	10^{-3}	10^{-2}	10^{-1}	1	10^1	10^2	10^3	10^4

The material parameters span a large relaxation spectrum to model the mechanical behavior of the polymer realistically. Those viscoelastic processes, for which the relaxation time τ_i is larger than 10^4 seconds, can be assumed to be inactive within the present time scale.

Contact modeling

The frictionless contact between the cylinders is modeled as a hard contact with finite sliding. The pure master-slave kinematic contact algorithm is used to enforce the mechanical contact constraints. In a hard contact, the surfaces transmit pressure only if the nodes of the slave surface (upper cylinder) contact the master surface (lower cylinder). Penetration of the surfaces is not allowed and there is no limit for the magnitude of the contact pressure that is transmitted. The finite sliding formulation allows for arbitrary separation, sliding and rotation of the surfaces.

The implemented kinematic contact algorithm is a prediction/correction process which, in general, progresses as follows:

i) Regarding the current increment, the kinematic state of the model is advanced into a predicted configuration without considering the contact conditions.

ii) It is determined which slave nodes penetrate the master surface.

iii) The depth of the node penetrations, the associated masses, and the time increment are used to calculate the resisting forces required to counteract the penetrations, that is, had they been added before the increment, no penetration would have occurred between the surfaces.

iv) The masses and the resisting forces related to the slave nodes are applied on the master surface to calculate an acceleration correction for it. Then, acceleration corrections are determined for the slave surface nodes based on the predicted penetrations, the time increment, and the corrections calculated for the master surface. These corrections are used to obtain a corrected configuration in which the contact constraints are enforced.

Computational details

The computations are performed by using ABAQUS/Explicit. For the equations presented in this section, see [22]. To calculate the response of a system, ABAQUS utilizes explicit central-difference based time integration. Accelerations are computed at the start of an increment by

$$\ddot{u}_{(i)} = M^{-1} \left(F_{(i)} - I_{(i)} \right) \ , \tag{3}$$

where M is the diagonal element mass matrix, F is the vector of externally applied forces and I is the vector of internal forces. Velocities and displacements are computed by

$$\dot{u}_{(i+1/2)} = \dot{u}_{(i-1/2)} + \frac{\Delta t_{(i+1)} + \Delta t_{(i)}}{2} \ddot{u}_{(i)} \tag{4}$$

$$u_{(i+1)} = u_{(i)} + \Delta t_{(i+1)} \dot{u}_{(i+1/2)} \ . \tag{5}$$

After this, the element level calculations are performed and then the next incremental step is taken. The method is explicit in the sense that the kinematic state is advanced using values of $\dot{u}_{(i-1/2)}$ and $\ddot{u}_{(i)}$ based on the previous increment.

In the explicit method, each increment is computationally inexpensive, because there are no simultaneous equations to be solved. An estimate for the stable time increment is

$$\Delta t_{stable} \approx \frac{L_{min}}{c_d} \ , \tag{6}$$

where L_{min} is the smallest element dimension in the mesh and the dilational wave speed is

$$c_d = \sqrt{\frac{\lambda + 2\mu}{\rho}} \ , \tag{7}$$

where λ and μ are Lame constants, and ρ is the density of the material. With a dense mesh, Eq. (6) typically results in very small time increments. Therefore, the explicit method is naturally suitable for achieving high resolution solutions for high-speed transient dynamic events, especially, if contact conditions causing extreme discontinuities are included.

For accuracy considerations, the energy balance of the model is investigated. Comparing the energy components of the model, it can be determined whether the analysis is giving physically reasonable results. The total energy expression used in ABAQUS, which should be a constant (zero), for the model is

$$E_{TOT} = E_E + E_{CD} + E_V + E_{KE} - E_W - E_{PW} \ , \tag{8}$$

where E_E is the strain energy, E_{CD} is the energy dissipated by viscoelasticity, E_V is the viscous dissipated energy, E_{KE} is the kinetic energy, E_W is the work of external forces and E_{PW} is the work of contact penalties. Generally, there is a small error in E_{TOT} in a numerical model. Large errors imply that the time increment is too large and causes instability, or the mesh is not dense enough. However, note that the energy inspection does not completely replace a mesh convergence study.

The studied model can be decomposed efficiently into eight domains, which allows the use of parallel computing. The memory requirements in the explicit method are very low, due to the absence of a global stiffness matrix required in implicit methods, in particular. Numerical computations are performed using an up-to-date Windows workstation and HP CP4000 BL ProLiant supercluster at CSC. With the current model, one second of simulation takes about five hours. Cluster computing allows one to perform multiple simultaneous computer runs, but does not increase the simulation speed as the model cannot be divided efficiently into more than eight domains.

By default, ABAQUS uses artificial bulk viscosity damping to introduce some damping into an explicit model. However, in this study the bulk viscosity has been set to zero. Damping is included in the model via the viscoelasticity of the polymer cover and the discrete dashpot of the upper cylinder.

Results

In the computations, the total mass of the upper cylinder was 572 kg and the parameter values for the support stiffness and damping were set to $k = 51.8$ MN/m and $c = 84$ Ns/m, respectively. Fig. 3 shows the vertical displacement of the upper cylinder in a simulation run. The cylinder is accelerated from rest to an angular velocity of $\omega = 100$ rad/s using a linear ramp in the time interval $0 - 5$ s. In the interval $5 - 55$ s, a smaller angular acceleration is applied and after 55 s the angular velocity $\omega = 146.1$ rad/s ($f_r = \omega/2\pi = 23.25$ Hz) is held constant. After the contact has been created during the first two seconds, the vertical force at the center of the upper cylinder is $F = 50$ kN and the vertical displacement of the upper cylinder is 70 μm. Evidently, the size of the contact area between the cylinders has an effect on the eigenfrequency of the system. With the created nip compression the eigenfrequency for the vertical vibration of the upper cylinder is $f_n = 210$ Hz.

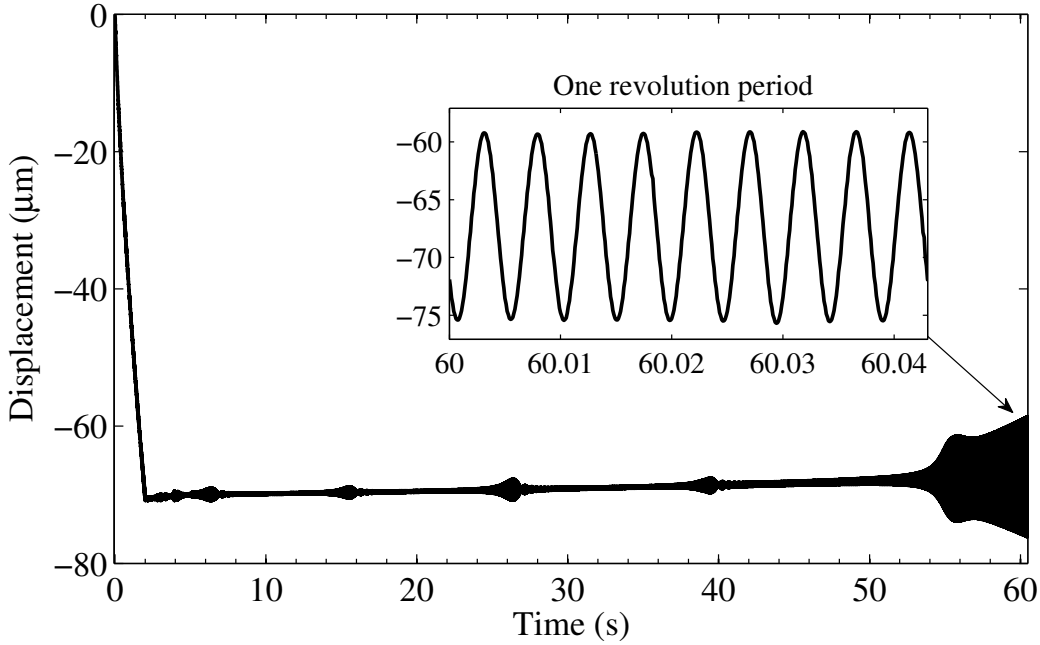

Figure 3. Vertical displacement response of the upper cylinder. Within the time intervals $0 - 5$ s, $5 - 55$ s and $55 - 60.5$ s, the angular accelerations $\alpha = 20$ rad/s^2, 0.922 rad/s^2 and 0 are used, respectively.

It can be seen from Fig. 3 that there are angular velocity ranges in which the vibration amplitude of the cylinder increases quickly, that is, strong barring appears. Fig. 4 shows a waterfall plot computed using the displacement signal from the time interval $5 - 55$ s. Fig. 4 shows that there is an amplitude peak in the vicinity of $f = 210$ Hz corresponding to the strong barring velocity ranges, indicating that the system is in resonance. We can define a polygonal number $N_i = f/f_r$ which gives essential information on the deformation pattern of the polymer cover. The pattern is evidently linked to the vibration frequency of the system – the long-term shape of the pattern is determined by the number of vibration periods of the upper roll in one revolution period. At $t = 60$ s the polygonal number is $N_9 = f/f_r = 210/23.25 = 9$. It can be seen from Fig. 4 that all the polygonal shapes seem to co-exist, however, only one is dominant at a time.

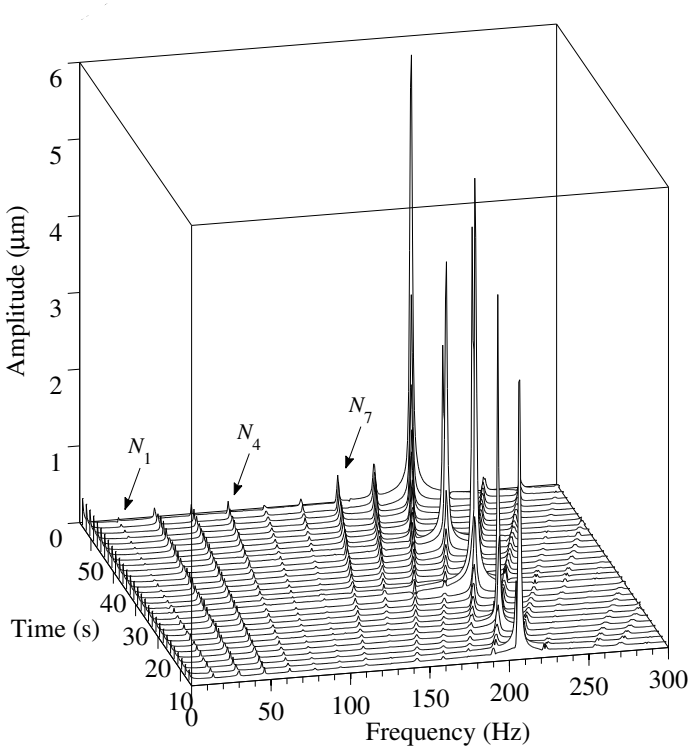

Figure 4. Waterfall plot computed by FFT from the displacement signal of Fig. 3 in the time interval $5 - 55$ s. The amplitude peak appears at 210 Hz corresponding to the eigenfrequency of the system. Thus, the system is in barring resonance.

The energy balance of the model is investigated briefly in Fig. 5 based on the simulation of Fig. 3. The relative error in E_{TOT} stays under 0.1 % at all times, thus the numerical analysis yields physically feasible results.

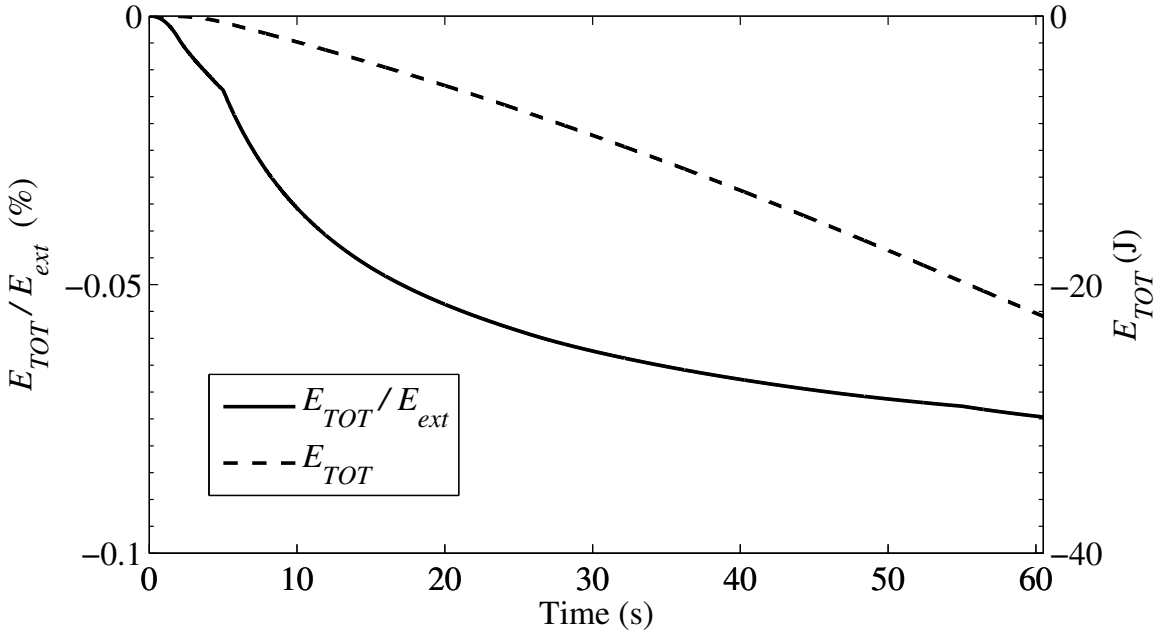

Figure 5. Energy balance of the system based on the simulation of Fig. 3. The numerical errors are small, therefore, the model produces realistic results. Here $E_{ext} = E_W + E_{PW}$ is the total external work done on the system (see Eq. (8)).

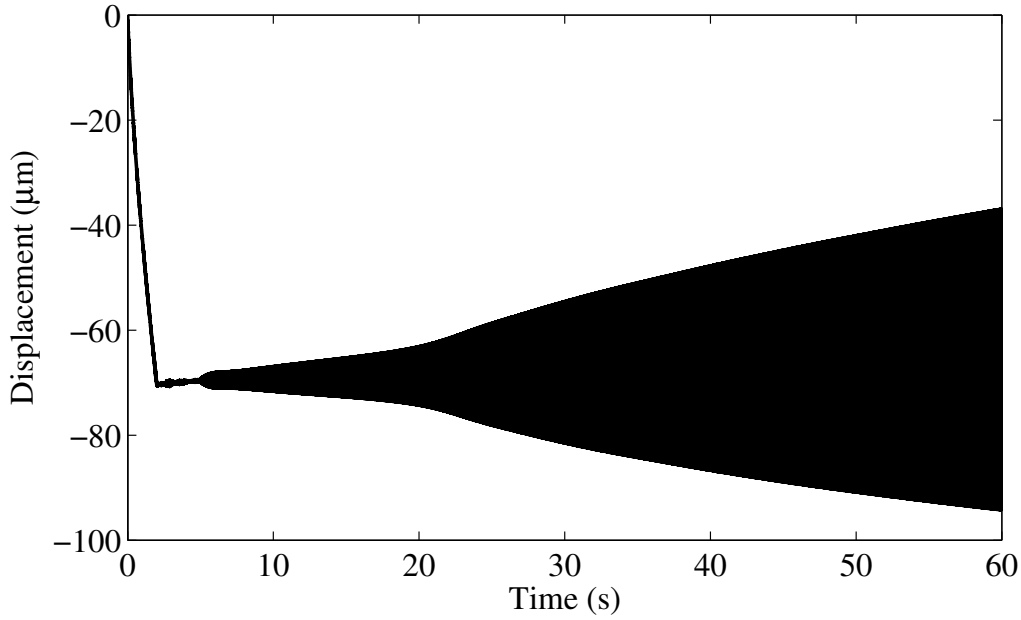

Figure 6. Vertical displacement response of the upper cylinder. The angular velocity achieves the value 146.1 rad/s at $t = 5$ s after which it remains constant. This value corresponds to the polygonal number $N_9 = 9$ and leads to a strong resonance.

Fig. 6 shows the displacement response of the upper cylinder as it is accelerated from rest to an angular velocity of $\omega = 146.1$ rad/s in five seconds and after this the angular velocity is held as constant. In the time interval $7-17$ s the vibration amplitude increases in a linear manner, after which there is a fast exponential type increase for a short period of time, then the amplitude continues to increase steadily at a lower pace.

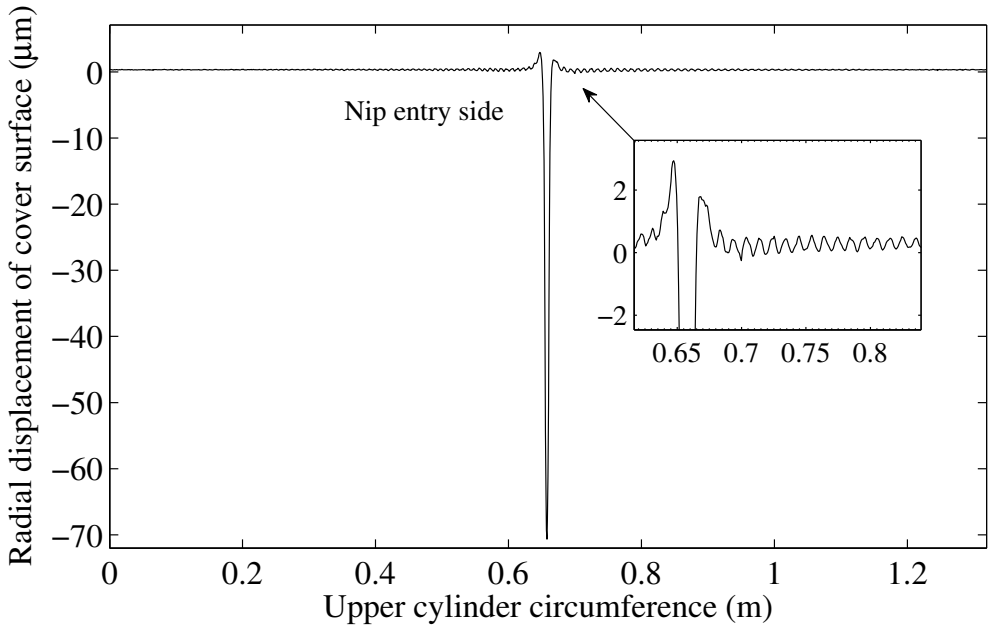

Figure 7. Radial displacement of the surface of the polymer cover. Nip waves are generated by a strong and sudden deformation of the cover when entering or leaving the nip.

The deformed shape of the polymer cover during the simulation of Fig. 6 is studied in Figs. 7 and 8 which show the radial displacement of the surface of the polymer cover. Fig. 7 shows the cover surface at $t = 6$ s. As can be seen in Fig. 7, the polymer cover exhibits a strong deformation in the nip which creates an interesting wavefront advancing to both directions from the nip at the speed of sound (dilation wave) in the polymer. The effect of these nip waves on barring vibrations is not yet known. Fig. 7 shows that there is a large compression in the middle of the nip, where as, on the edges of the nip the cover extrudes. It is notable that the superposition of these compressions and extensions determines the development of the cover deformation pattern in the long run. The extensional deformation is also affected by the centrifugal force acting on the polymer cover.

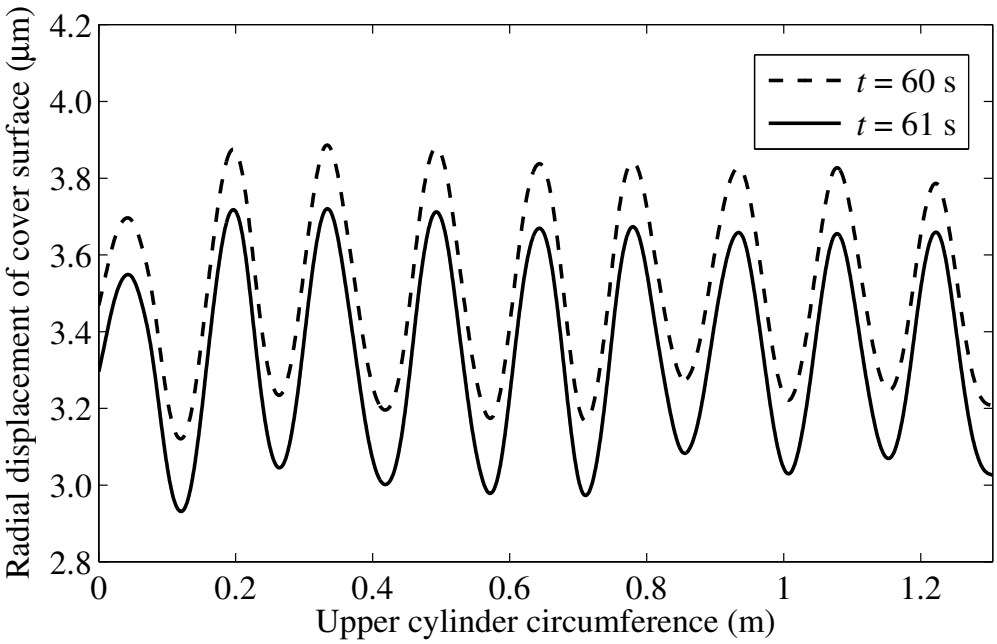

Figure 8. Wave-like polygonal deformation pattern on the polymer cover generated by barring. The relaxation of the polymer is a long-term process.

In the simulation run shown in Fig. 6, the contact between the cylinders is removed at $t = 60$ s and the angular velocity is decreased to zero using a linear ramp within the time interval $60 - 61$ s. Fig. 8 shows clearly that the deformation pattern generated by barring consists of nine sinewave-like humps. It can be seen that within the time interval $60 - 61$ s the average radial displacement of 3.5 μm of the cover surface decreases by about 0.15 μm, while the wave-like deformation pattern itself remains practically unchanged. This shows that the wave pattern in this case is mainly due to slower relaxation processes, for which the relaxation times are clearly longer than 1 s.

Fig. 9 shows an amplitude versus angular velocity plot for the vertical vibration of the upper cylinder, which has been created from separate simulations performed in the same way as the one in Fig. 6. The amplitudes have been measured at two instances, $t = 12$ and 15 s, that is, within the zone of the linear increase in amplitude. The amplitude curves display a peak in the vicinity of $\omega = 146$ rad/s as a result of a resonance condition created in the system.

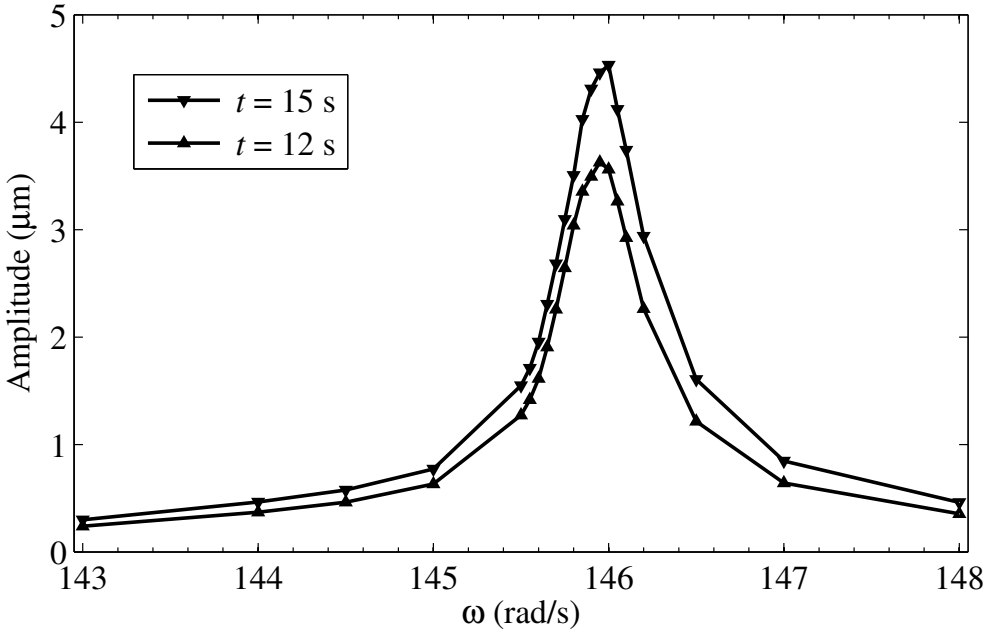

Figure 9. Amplitude plot of the vertical vibration combined from separate simulations. The barring mechanism creates a resonance condition in the system, seen as an amplitude peak in this figure.

Conclusions

In this study, the barring vibration phenomenon caused by a viscoelastic polymer cover in a rolling contact system was studied by using a finite element approach. Up-to-date finite element softwares provide suitable tools for this purpose.

By using a two-dimensional FE model, it was shown that strong self-excited barring vibration is a result of a resonance condition in a rolling contact system. In the long run, barring leads to the formation of a sinewave-like deformation pattern on the polymer-covered cylinder. By using a FE model, the existence of nip waves radiated from the nip in both directions was discovered. The barring resonance condition will be investigated in detail in further studies.

Acknowledgements

We acknowledge CSC − IT Center for Science Ltd. for the allocation of computational resources.

References

[1] P.R Nayak, Contact vibrations, *Journal of Sound and Vibration*, 22 (3) (1972) 297-322.

[2] G.G. Gray, K.L. Johnson, The dynamic response of elastic bodies in rolling contact to random roughness of their surfaces, *Journal of Sound and Vibration*, 22 (3) (1972) 323-342.

[3] K.L. Johnson, *Contact Mechanics*, Cambridge University Press, Cambridge, 1987.

[4] J.J. Kalker, *Three-Dimensional Elastic Bodies in Rolling Contact*, Kluwer Academic Publishers, Dordrecht, 1990.

[5] L. Nasdala, M. Kaliske, A. Becker, H. Rothert, An efficient viscoelastic formulation for steady-state rolling structures, *Computational Mechanics*, 22 (5) (1998) 395-403.

[6] J.A. González, R. Abascal, Efficient stress evaluation of stationary viscoelastic rolling contact problems using boundary element method: Application to viscoelastic coatings, *Engineering Analysis with Boundary Elements*. 30 (6) (2006) 426-434.

[7] M. Ziefle, U. Nackenhorst, Numerical techniques for rolling rubber wheels: treatment of inelastic material properties and frictional contact, *Computational Mechanics*, 42 (3) (2008) 337-356.

[8] A.T. Karttunen, R. von Hertzen, Polymer cover induced self-excited vibrations of nipped rolls, *Journal of Sound and Vibration*, 330 (16) (2011) 3959-3972.

[9] A. Sueoka, T. Ryu, T. Kondou, Y. Tsuda, K. Katayama, K. Takasaki, M. Yamaguchi, H. Hirooka, Polygonal deformation of roll-covering rubber, *JSME International Journal, Series C*, 39 (1) (1996) 1-10.

[10] A. Sueoka, T. Ryu, M. Yoshikawa, T. Kondou, Y. Tsuda, Pattern formation generated in a winder system of textile machine, *JSME International Journal, Series C*, 41 (3) (1998) 630-638.

[11] M. Jorkama, R. von Hertzen, Delay phenomena in roll vibrations, *Proceedings of the VIII Finnish Mechanics Days*, June 2003, Espoo, Finland, pp. 111-121.

[12] M. Jorkama, R. von Hertzen, Two-drum winder stability analysis, *Pulp & Paper Canada*, 108 (5) (2007) 35-37.

[13] L.H. Yuan, Analysis of delay phenomena in roll dynamics, *Doctoral Thesis*, Tampere University of Technology, 2002.

[14] L.H. Yuan, V.-M. Järvenpää, Nonlinear vibrations in a covered roll system with viscoelastic contact, *Communications in Nonlinear Science and Numerical Simulation*, 14 (7) (2009) 3170-3178.

[15] F. Chinn, Dynamic instability of poly covered press rolls, *Pulp & Paper Canada*, 100 (1) (1999) 11-14.

[16] T. Vuoristo, V.-T. Kuokkala, E. Keskinen, Dynamic compression testing of particle-reinforced polymer roll cover materials, *Composites: Part A*, 31 (8) (2000) 815-822.

[17] T. Vuoristo, V.-T. Kuokkala, Creep, recovery and high strain rate response of soft roll cover materials, *Mechanics of Materials*, 34 (8) (2002) 493-504.

[18] N. Sowa, T. Kondou, H. Mori, M.S. Choi, Method of preventing unstable vibration caused by time delays in contact rotating systems (application of new stability analysis), *JSME International Journal, Series C*, 49 (4) (2006) 973-982.

[19] K. Matzusaki, A. Sueoka, T. Ryu, H. Morita, Generation mechanism of polygonal wear of work rolls in a hot leveler and a countermeasure by dynamic absorbers, *International Journal of Machine Tools and Manufacture*, 48 (9) (2008) 983-993.

[20] K. Matzusaki, A. Sueoka, T. Ryu, H. Morita, K. Hidaka, S. Noguchi, Polygonal wear of work rolls in a hot leveler of a steel making machine (4th Report, Experimental verification of a countermeasure by using dynamic absorbers), *Journal of Environment and Engineering*, 3 (1) (2008) 146-157.

[21] T. Ryu, K. Matzusaki, A. Sueoka, H. Morita, Countermeasures against pattern formation phenomena of thin sheet winder by using dynamic absorbers, *Journal of System Design and Dynamics*, 3 (5) (2009) 814-826.

[22] Dassault Systemes Simulia Corp., Abaqus 6.10 Theory Manual, 2010, Providence, RI.

Anssi T. Karttunen, Raimo von Hertzen
Aalto University School of Engineering, Department of Applied Mechanics
P.O. Box 14300, FI-00076 Aalto, Finland
anssi.karttunen@aalto.fi, raimo.von.hertzen@aalto.fi